FATIGUE FRACTURE IN LANDING GEAR STEELS

R.J.H. Wanhill
National Aerospace Laboratory NLR
Amsterdam, The Netherlands

ICAS-86-4.9.3

Abstract

Characteristics of fatigue and overload fracture in high strength steel landing gear forgings were investigated. Fatigue fracture was typified by microserrated acicular ridges (misars) and to a lesser extent by fatigue striations. Overload fracture was by microvoid coalescence (dimples). After severe corrosion due to outdoor exposure it was still possible to identify fatigue fracture, but overload dimples were much less evident.

Constant amplitude fatigue crack growth data were used to predict crack growth under block programme flight-by-flight loading. The predictions were made using a characteristic-K approach and were compared with test data. The results were encouraging for analytical estimation of service failure crack growth lives.

Introduction

Aircraft landing gears consist mostly of highly loaded nonredundant components with severe constraints on weight and space. For these reasons many components are made from high strength low alloy steels. During manufacture much effort is made to ensure defect-free components. Nevertheless, undetectable damage or material defects may be present. Also, service operation can result in mechanically and environmentally induced damage.

Fatigue cracks may initiate from the various kinds of damage or defects. Once initiated the fatigue cracks usually propagate to cause component failure, since stresses are high and there is little or no redundancy. In turn, component failure may lead to operational failure of the entire landing gear.

Operational failure is accompanied by much mechanical damage and additional component failures due to overload. Failure investigation must therefore distinguish between fatigue and overload failures. For high strength steels this is by no means an easy task, for three reasons:

1. The types of fracture occurring in fatigue may not be unambiguously relatable to fatigue. Examples are intergranular fracture and microvoid coalescence, which can also occur during overload failure.

2. Features characteristic of fatigue fracture may be partially or completely obliterated by environmental attack (rusting, hydraulic fluid) and mechanical damage during operational failure.

3. The amount of fatigue fracture before component failure is often very limited, since stresses are high and fracture toughnesses relatively low.

With the foregoing considerations in mind the test programme outlined in Table 1 was carried out. The main purpose of this programme was to provide guidelines for distinguishing between fatigue and overload failures of high strength steel landing gear components. For this purpose constant amplitude fatigue loading was judged to be most suitable. However, since estimates of fatigue crack propagation lives for service failures are frequently desired, the feasibility of doing this fractographically and analytically was checked by including tests with approximate flight-by-flight loading.

● **MATERIALS**	D6AC, 4330V, 300M steel forgings
● **SPECIMENS**	Standard compact-type (CT)
● **FATIGUE LOADINGS**	1. Constant amplitude 2. Block programme flight–by–flight
● **ENVIRONMENTS**	1. Fatigue in laboratory air 2. Outdoor exposure of fracture surfaces
● **EXAMINATION**	Fractography and metallography
● **OBJECTIVES**	1. Characterization of fatigue and overload fractures 2. Influence of exposure on fracture surface appearance 3. Fractographic and metallographic correlations 4. Detection of flight–by–flight fracture surface markings 5. Correlation of fatigue crack growth rates under constant amplitude and flight–by–flight loading 6. Comparison of predicted flight–by–flight fatigue crack growth curves with test data

Table 1 Test Programme Overview

Materials and Specimens

The materials were D6AC, 4330V and 300M low alloy steel forgings from a fighter aircraft main landing gear, see Figure 1. Chevron notched compact-type (CT) specimens per ASTM Standard E 647 were machined from the forgings before heat treatment. All specimens were oriented with the loading direction parallel to principal loading directions in the original components. The specimens were heat treated according to MIL-H-6875 into the following ranges of ultimate tensile strength: D6AC and 4330V (1517-1655 MPa); 300M (1860-1931 MPa).

At this point the selection of steels and strength levels will be briefly discussed. 300M is widely used in landing gear components requiring high tensile strength, for example the tension strut shown in Figure 1. The achievable strength range enables this material to give the highest strength/weight ratio of any commercially available low alloy steel suitable for landing gear.

When other factors such as stiffness and thickness control the design of components it is possible to use lower strength ranges without weight penalties. The selection of a steel then depends on other considerations. For example, D6AC

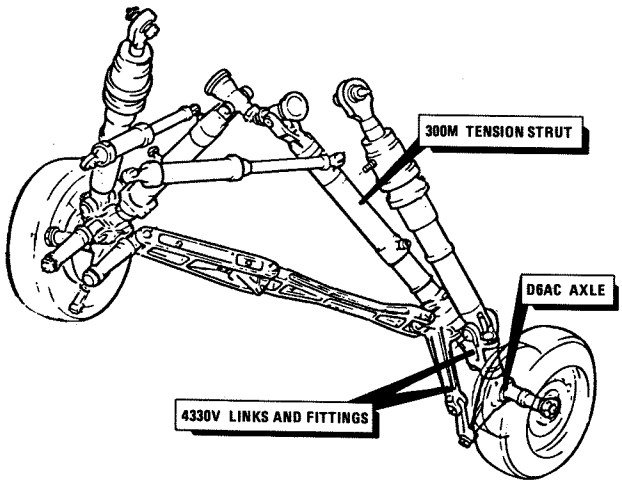

Figure 1 Main Landing Gear

is deeply hardenable and suitable for heavy sections. It is also heat resistant, which is an advantage for axles because considerable heat is generated during braking. On the other hand, 4330V is easier to forge into complex shapes, two of which are shown in Figure 1.

Experimental Procedure

The CT specimens were fatigued in laboratory air at room temperature. There were two types of fatigue loading:

1. Constant amplitude with load ratio R = P_{min}/P_{max} of 0.1 and cycle frequency 66-150 Hz.

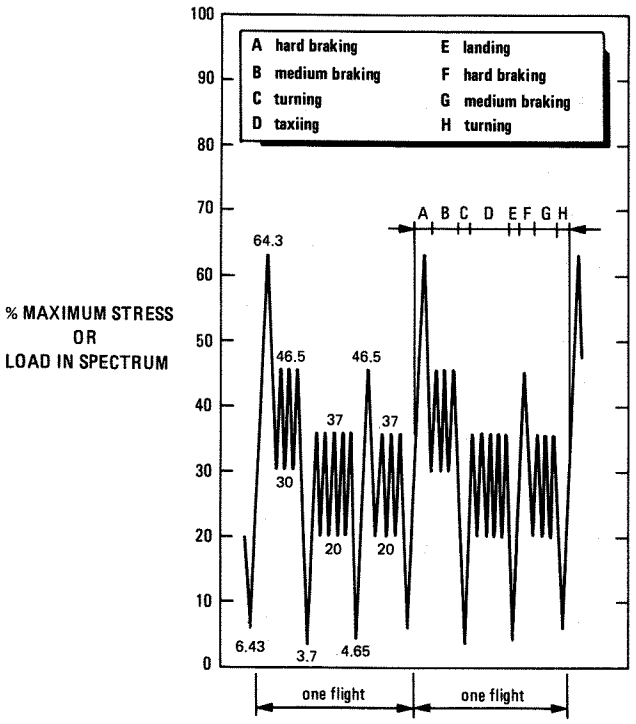

Figure 2 Block Programme Flight-by-Flight Loading

2. Block programme flight-by-flight loading with a nominal cycle frequency of 25 Hz.

The block programme is shown in Figure 2. It is a simplified version of the load histories developed in references (1) and (2).

Crack growth was measured optically. After testing the specimens were broken open. One half of each specimen was examined fractographically and metallographically in the as-tested condition. The remaining halves were exposed outdoors for 100 hours before examination. During this period the weather conditions included temperatures between 265-285 K and intermittent precipitation, mostly rain. The fracture surfaces exhibited extensive rust spotting with apparently clean areas in between.

Crack Growth Rates

Fatigue crack propagation rates were obtained from increments of crack growth:

$$\frac{da}{dn} = \frac{a_{i+1} - a_i}{n_{i+1} - n_i} \qquad (1)$$

and were correlated with $a^* = (a_{i+1}+a_i)/2$, which is the mean of the growth interval.

Stress intensity factors were calculated from the following expression:

$$K = \frac{P}{B\sqrt{W}} \frac{(2+\alpha)}{(1-\alpha)^{3/2}} (0.886 + 4.64\alpha - 13.32\alpha^2 + 14.72\alpha^3 - 5.6\alpha^4) \qquad (2)$$

where B is the specimen thickness, W is the width, and $\alpha = a/W$ where a is the crack length (see ASTM Standard E 647 for further details).

Constant Amplitude Data Correlation

The data are presented in Figure 3 together with data envelopes for many steels in two ranges of yield strength[3]. The present results fall within the lower envelope and there is little difference

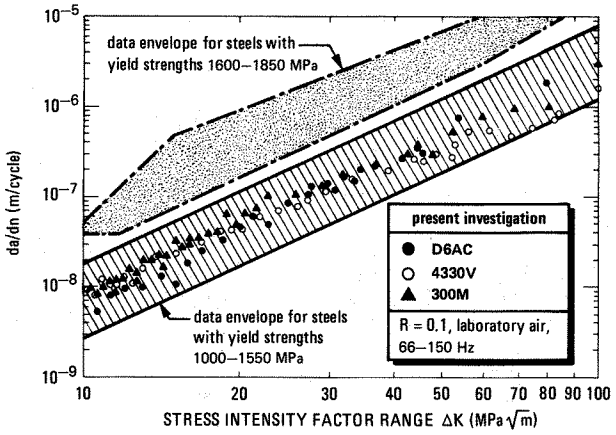

Figure 3 Constant Amplitude Crack Growth Rate Data

in crack growth rates. For D6AC and 4330V this is not surprising, since the heat treatments resulted in nominal yield strengths of 1300-1350 MPa. However, for 300M the nominal yield strength was at least 1600 MPa, so that significantly higher crack growth rates were expected.

The present data were well represented by the "Paris Law" with the parameters given in Table 2. The values of m are particularly significant. It has been shown that m = 3 implies better fracture toughness and absence of purely tensile fracture during fatigue[4].

FOR R = 0.1, $\frac{da}{dn} = C(\Delta K)^m$		
MATERIAL	C	m
D6AC	7.18×10^{-12}	2.86
4330V	5.49×10^{-11}	2.20
300M	2.46×10^{-11}	2.55

Table 2 "Paris Law" Parameters for the Constant Amplitude Crack Growth Rate Data Correlated by ΔK

Block Programme and Constant Amplitude Data Correlation by a Characteristic-K Approach

Root mean (rm) ΔK values were used to correlate the block programme and constant amplitude fatigue crack growth data. The general expression for ΔK_{rm} is

$$\Delta K_{rm} = \sqrt[m']{\frac{\Sigma (\Delta K_i)^{m'} n_i}{\Sigma n_i}} \qquad (3)$$

where n_i is the number of load excursions corresponding to ΔK_i; m' is the slope of the constant amplitude log da/dn versus log ΔK_{eff} plot; and ΔK_i is derived from estimates of K_{opi} and the following equations:

$$\left.\begin{aligned} (\Delta K_i)^{m'} &= (K_{maxi}-K_{opi})^{m'} - (K_{mini}-K_{opi})^{m'} \\ &\qquad \text{for } K_{opi} < K_{mini} \\ &= (K_{maxi}-K_{opi})^{m'} \quad \text{for } K_{opi} \geq K_{mini} \end{aligned}\right\} \qquad (4)$$

Equations (4) were derived by De Koning[5] and are compatible with the successful method of cycle counting known as "rainflow" or "range-pair-range"[6]. Note also that for constant amplitude loading $\Delta K_i = \Delta K_{eff} = \Delta K_{rm}$.

Estimates of K_{opi} were obtained as follows. For constant amplitude loading with R = 0.1 a reliable estimate of K_{opi} for high strength steels is given in reference (7). It was found that $K_{opi} = 0.19\ K_{maxi}$ over a wide range of ΔK. Thus for the constant amplitude tests in this investigation it was assumed that $\Delta K_{rm} = \Delta K_i = 0.81\ K_{maxi} = 0.9\ \Delta K$. This also means that there was no change in slope parameter, i.e. m = m'.

For block programme loading K_{opi} was estimated from comparisons of calculated relative spacings of fatigue striations using equations (4) and fractographic measurements. In theory this can be done in two ways:

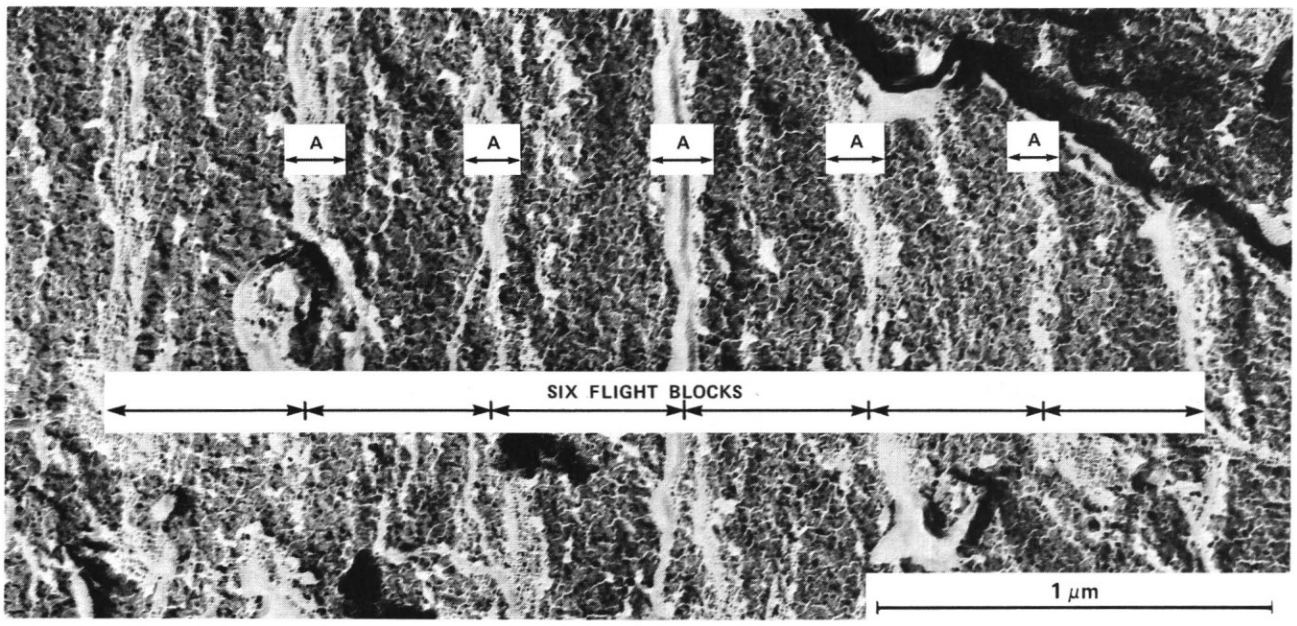

Figure 4 Fatigue Striation Marks for Block Programme Loaded 4330V Steel: Transmission Electron Fractograph of a Two-Stage Replica at 0^o Tilt

1. Assume K_{opi} to be constant during the flight block. Choose several hypothetical K_{opi} levels and calculate the relative spacings of fatigue striations in a flight block. Compare calculated and actual relative striation spacings and flight block lengths to obtain a best fit and hence an estimate of K_{opi}.

2. Assume a value of K_{opi} for one or more load excursions and derive other K_{opi} value from the actual relative spacings of fatigue striations in a flight block.

In fact, even at very high magnifications only the flight blocks and the largest striations corresponding to the upward load excursion in segment A of the flight block (see Figure 2) could be identified. This is illustrated in Figure 4. On this basis it was assumed that K_{opi} was effectively constant during the flight block. With this assumption the relative widths of the largest striations and the flight blocks could be used to estimate K_{opi}. On average the largest striations accounted for slightly less than 30 % of the flight block widths. This corresponded to K_{opi} = 26 % of the maximum stress intensity factor in the flight block, i.e. the stress intensity factor for the peak load in segment A. This K_{opi} value was then substituted into equations (4) to obtain ΔK_i values for each load excursion. These ΔK_i values were substituted into equation (3) to obtain ΔK_{rm}.

Figure 5 shows the block programme and constant amplitude fatigue crack growth rates plotted against ΔK_{rm}. The use of ΔK_{rm} resulted in a good correlation of the data.

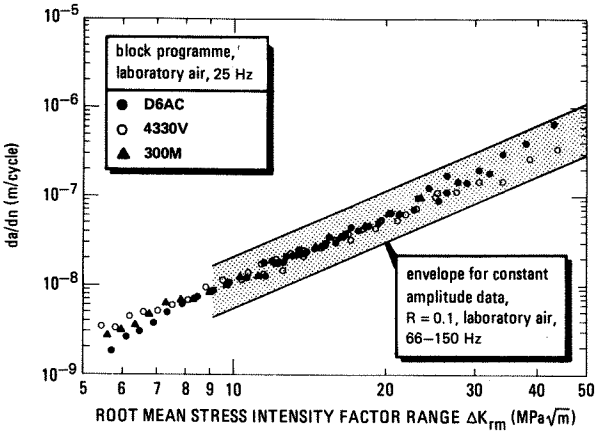

Figure 5 Correlation of Block Programme and Constant Amplitude Crack Growth Rate Data by ΔK_{rm}

Fractographic and Metallographic Examination

A review of the fractographic and metallographic results is given in Table 3. These results will be discussed in more detail in the following subsections.

TYPE OF FRACTURE	FRACTOGRAPHIC CHARACTERISTICS	COMMENTS
FATIGUE	• ΔK_{rm} 6–10 MPa$\sqrt{m}$ – microserrated acicular ridges (misars) – isolated intergranular facets (prior austenite grain boundaries) • ΔK_{rm} 10–20 MPa$\sqrt{m}$ – "rounding" of misars – striations depicting flight blocks (not individual cycles) • ΔK_{rm} 20–40 MPa$\sqrt{m}$ – some irregular striations	• misars correlate with tempered martensite needles and are most characteristic except at high ΔK_{rm} • 100 hours outdoors left fairly clean isolated areas with misars particularly identifiable, even though macroscopically the fracture surfaces appeared completely rusted
OVERLOAD	microvoid coalescence (dimples)	100 hours outdoors made it much less evident that failure was overload by microvoid coalescence

Table 3 Summary of the Fractographic and Metallographic Results

Fatigue Fracture

The fatigue fracture surfaces were examined by scanning electron microscopy at several ΔK_{rm} levels. The fractographic appearances were very similar for all three steels under the same type of loading at each ΔK_{rm} level. Also, the fractographic appearances at lower magnifications ($\leq$ 1000X) were similar when ΔK_{rm} for constant amplitude loading was about twice that for block programme loading. Examples are given in Figure 6.

The following trends were observed:

1. For ΔK_{rm} values of 6 MPa$\sqrt{m}$ (block programme) and 10 MPa$\sqrt{m}$ (constant amplitude) the fatigue fracture surfaces consisted mainly of microserrated acicular ridges (misars) with isolated intergranular facets. Fatigue striations were not resolvable.

2. For ΔK_{rm} values of 10 MPa$\sqrt{m}$ (block programme) and 20 MPa$\sqrt{m}$ (constant amplitude) examination at higher magnification revealed subtle "rounding" of the misars, most probably owing to increased crack tip plasticity, and fatigue striation marks on fracture surfaces produced by block programme loading. These are illustrated in the middle column/bottom row of Figure 6.

3. For ΔK_{rm} values of 20 MPa$\sqrt{m}$ (block programme) and 40 MPa$\sqrt{m}$ (constant amplitude) the typical misar appearance was no longer identifiable, but striations were visible on fracture surfaces produced during both constant amplitude and block programme loading. However, the striations were often irregular, which detracts from their diagnostic usefulness since they then resemble stretch and tear markings.

The fatigue striation marks for block programme loading were wider than those for constant amplitude loading although, as may be ascertained from figure 5, the cyclic crack growth rate was lower. The explanation is that the fatigue striation marks for block programme loading represented flight blocks, not individual cycles. This is also the reason why striation marks at lower ΔK_{rm} values were visible only for block programme loading.

4. Outdoor exposure resulted in extensive but discontinuous corrosion (rusting) with fairly clean

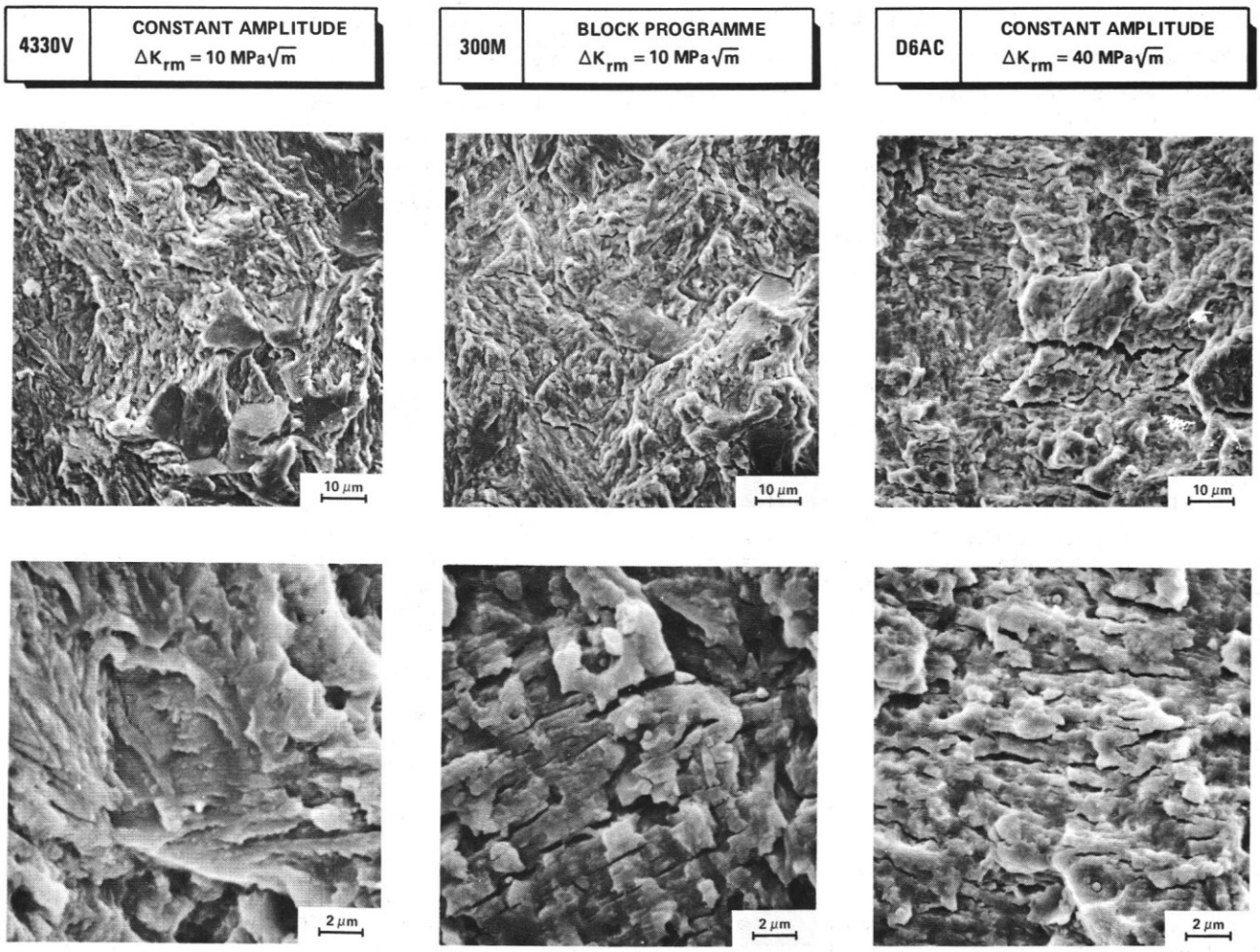

Figure 6 Examples of Fatigue Fracture Characteristics for All Three Steels

areas in between. In these clean areas misars, intergranular facets and fatigue striations were identifiable, particularly the misars.

Overload Fracture

For all three steels the overload fracture surfaces were covered by a mixture of small and large dimples formed by microvoid coalescence. This is a very distinctive type of fracture. However, outdoor exposure made it far less evident, as can be seen in Figure 7.

Fractographic and Metallographic Correlations

Metallographic sections parallel to the macroscopic plane of fracture were prepared by standard techniques. All three steels had similar microstructures of tempered martensite needles with evidence of prior austenite grain boundaries. There

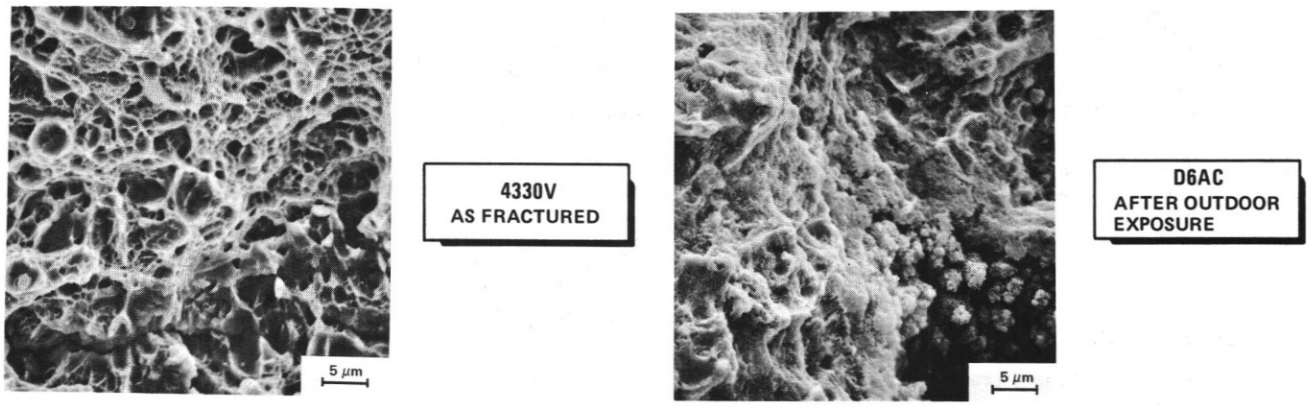

Fig. 7 Examples of Overload Fracture Characteristics

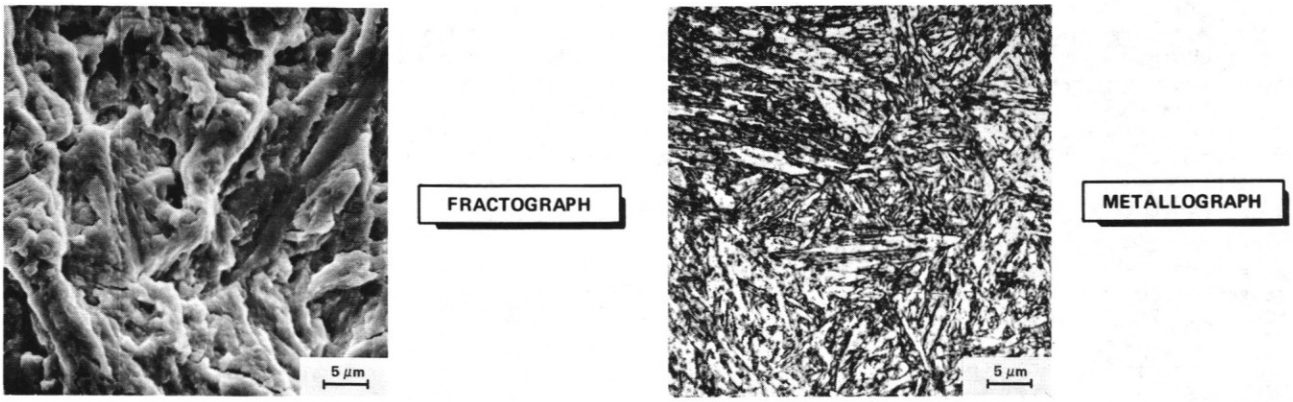

Fig. 8 Similar Morphology of Misars and Tempered Martensite Needles; 4330V Steel

were two fracture features that could be related directly to the microstructures:

1. The microserrated acicular ridges (misars) which had sizes and aspect ratios similar to those of the tempered martensite needles.

2. Isolated intergranular facets, corresponding to prior austenite grain boundaries.

Examples of the similarity of misars and tempered martensite needles, and hence most probably their correspondence, are given in Figure 8.

Crack Growth Predictions

Predictions of fatigue crack growth under block programme flight-by-flight loading were made by numerically integrating "Paris Law" approximations to the constant amplitude log da/dn versus log ΔK_{rm} (= log 0.9 ΔK) data and using for block programme loading the appropriate ΔK_{rm} values based on a constant K_{opi} = 26 % of the maximum stress intensity factor in the flight block.

Predictions Using Numerical Integration and ΔK_{rm}

The constant amplitude log da/dn versus log ΔK_{rm} data were approximated by the "Paris Law" with the parameters given in Table 4.

$\frac{da}{dn} = C'(\Delta K_{rm})^{m'}$		
MATERIAL	C'	m'
D6AC	9.70×10^{-12}	2.86
4330V	6.92×10^{-11}	2.20
300M	3.22×10^{-11}	2.55

Table 4 "Paris Law" Parameters for the Constant Amplitude Crack Growth Rate Data Correlated by ΔK_{rm}

Owing to the good correlation of block programme and constant amplitude fatigue crack growth rates by ΔK_{rm}, Figure 5, it was then assumed that the

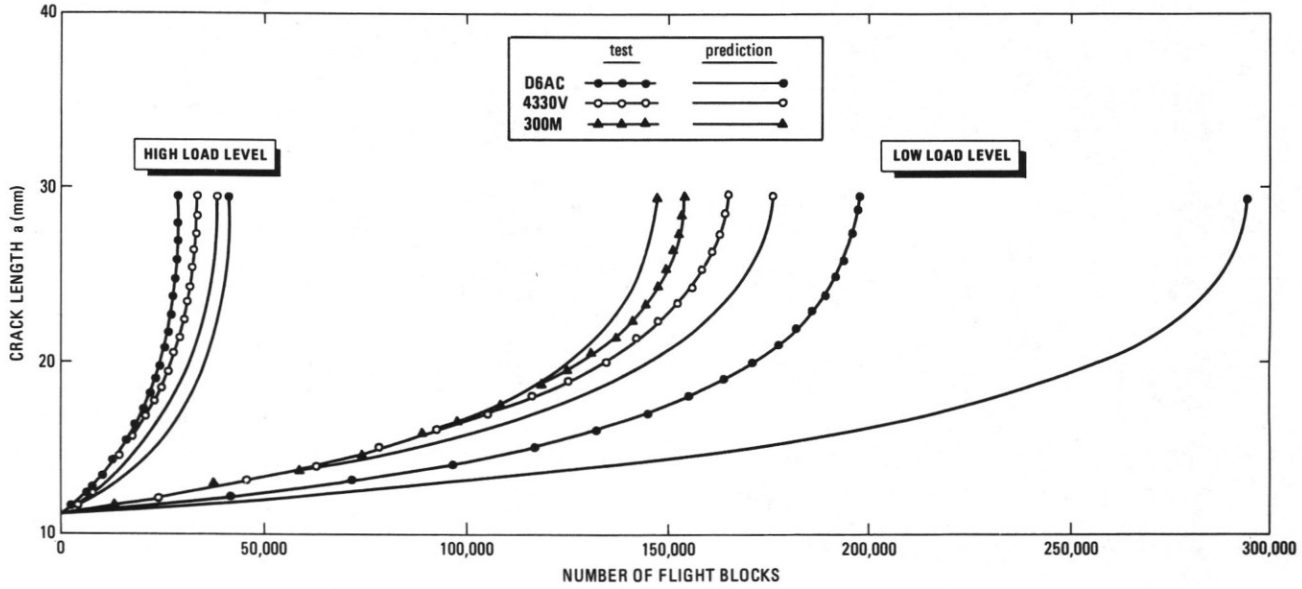

Figure 9 Comparison of Block Programme Loading Test Data and Predictions Using ΔK_{rm}

"Paris Law" approximations to the constant amplitude data were also valid for the block programme data: this is what one would have to do in practice if only constant amplitude data were available for predicting service life.

Next a number of da/dn values for various crack lengths were calculated by substituting appropriate ΔK_{rm} values in the "Paris Law" approximations. Plots were made of dn/da versus a. These plots were numerically integrated to obtain a versus n, converting cycles into flight blocks (each flight block is 13 cycles).

The predicted crack growth curves are compared with test data in Figure 9. Very good predictions were obtained for 4330V and 300M steels. The predictions for D6AC steel were unconservative by about 50 %. These results are still reasonable. They are also informative, as will be shown in the next section of this paper.

Discussion

Fatigue fracture was characterized by microserrated acicular ridges (misars) and striation marks, which were particularly visible for block programme (flight-by-flight) loading. The striations were often irregular, which detracts from their diagnostic usefulness and also their use in estimating service failure crack growth lives.

In the absence of corrosion the fatigue fractures were clearly distinguishable from overload fracture, which occurred by microvoid coalescence. However, after outdoor exposure resulting in extensive rust spotting the characteristic dimples of overload fracture were far less evident. Distinguishing between fatigue and overload fracture then relies mainly on identifying fatigue from misars and striation marks in locally cleaner areas.

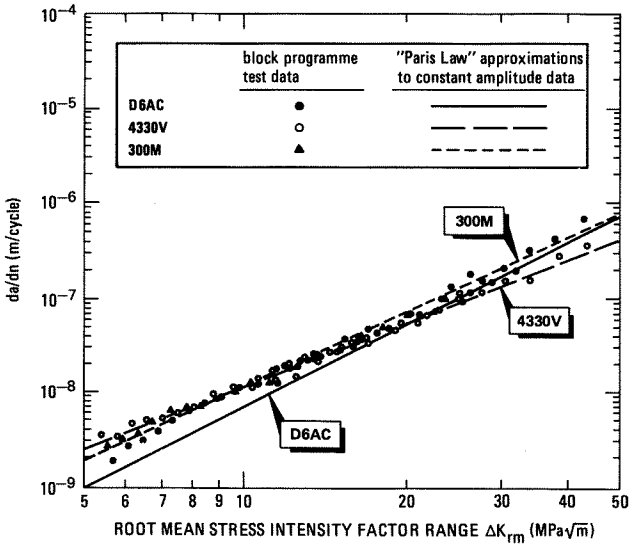

Figure 10 Comparison of Block Programme Crack Growth Rate Data and "Paris Law" Approximations to the Constant Amplitude Crack Growth Rate Data

Misars are especially useful for identifying fatigue fractures in high strength low alloy steels. They are readily found by scanning electron microscopy and occur widely. This is most probably because they represent cyclic deformation and fracture influenced locally by the presence of tempered martensite needles characteristic of the microstructures of such steels.

Block programme and constant amplitude fatigue crack growth rates were well correlated by root mean values of the stress intensity factor range, ΔK_{rm}. In the first instance this is encouraging for efficient prediction of crack growth lives under load histories containing peak loads with short recurrence periods that result in a regular, quasi-stationary crack growth process, as in the present investigation. However, the predictions strongly depend on the accuracy with which the "Paris Law" approximations to constant amplitude data also apply to crack growth under variable amplitude loading. This is illustrated by the comparison of test data and predictions in Figure 9 and the crack growth rate plots in Figure 10:

1. For 4330V and 300M steels the "Paris Law" approximations to the constant amplitude crack growth rate data fitted the block programme crack growth rate data very well, and very good predictions were obtained.

2. For D6AC steel the "Paris Law" approximation to the constant amplitude crack growth rate data underestimated the block programme crack growth rates at low ΔK_{rm} values, and this resulted in significantly unconservative predictions. In this case the predictions obviously can be improved by adjusting the "Paris Law" approximation to better fit the block programme crack growth rate data. But in practice there might be only constant amplitude data available.

The result for D6AC steel shows the necessity for caution in assessing variable amplitude fatigue crack growth lives using constant amplitude crack growth rate data and a characteristic-K (ΔK_{rm}) approach. For a best estimate the constant amplitude crack growth rate data should be obtained from as many sources as possible before fitting a "Paris Law" approximation. If a conservative estimate is required a "Paris Law" approximation can be fitted as an upper bound to the data. (Similar suggestions have been made by others).

Finally, the fact that fatigue fracture appearances at lower magnifications were similar when ΔK_{rm} for constant amplitude loading was about twice that for block programme loading can be explained as follows. The overall appearances of the fatigue fractures were probably controlled by the maximum extent of cyclic plasticity in the crack tip region. For constant amplitude loading the maximum extent of the cyclic plasticity is simply related to ΔK_{rm} ($= \Delta K_{eff}$) via an expression for the cyclic plastic zone size. However, for block programme loading the maximum extent of crack tip cyclic plasticity is determined by the largest load excursion per flight block. Accounting approximately for crack closure, i.e. assuming K_{opi} = 26 % of the maximum stress intensity factor in the flight block, resulted in ΔK_i for the largest load excur-

sion being about twice ΔK_{rm} for the flight block. Thus the fatigue fracture appearances at lower magnifications were similar when ΔK_{rm} for constant amplitude loading was about equal to ΔK_i for the largest load excursion in the flight block and therefore about twice ΔK_{rm} for the flight block.

This observation has an interesting implication which will be discussed using Figure 11. The constant amplitude fatigue crack growth rate curve for steels shows a transition down to an effectively zero growth rate (threshold) when the cyclic plastic zone size, r_p^c, becomes less than the grain size [8]. There is a concominant change in fatigue fracture from a continuum-type mechanism above the transition to faceted fracture below it [8,9].

Under variable amplitude load histories containing peak loads with short recurrence periods the transition to threshold may well be delayed until the maximum cyclic plastic zone size becomes less than the grain size, as shown in Figure 11. This means that despite good correlation of constant and variable amplitude fatigue crack growth rates by ΔK_{rm} over a wide range, as in the present investigation, it could be very unconservative to use below-transition constant amplitude data to predict variable amplitude fatigue crack growth at low stress intensities. Also, the constant amplitude threshold stress intensity factor range, ΔK_{th}, should not be used as a criterion for determining whether fatigue crack growth under variable amplitude loading can occur.

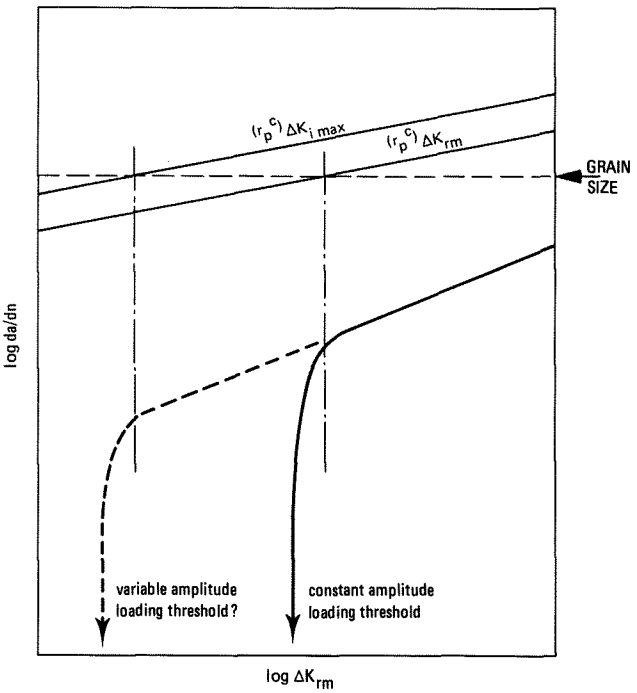

Figure 11 Schematic Fatigue Crack Growth Rate Curves at low ΔK_{rm}

Conclusions

Investigation of fatigue and overload fracture in high strength low alloy steel landing gear forgings has shown the following:

1. Fatigue fracture was characterized by microserrated acicular ridges (misars) and to a lesser extent by striation marks, which were more evident for block programme (flight-by-flight) loading. Regular fatigue striations were infrequent and it is unlikely that fractography will provide good estimates of service failure fatigue crack growth lives.

2. Uncorroded fatigue and overload fractures could readily be distinguished. Overload occurred by microvoid coalescence resulting in well-defined dimples.

3. After outdoor exposure resulting in extensive rust spotting the dimples characterizing overload fracture were far less evident. Distinguishing between fatigue and overload fractures then has to rely mainly on identifying fatigue from misars and striation marks.

4. Misars and intergranular facets on fatigue fracture surfaces correlated with the tempered martensite needles and prior austenite grain boundaries in the microstructures.

5. Block programme and constant amplitude fatigue crack growth rates were well correlated by root mean values of the stress intensity factor range, ΔK_{rm}.

6. Predictions of block programme fatigue crack growth curves were made using a characteristic-K (ΔK_{rm}) approach. The predictions agreed well with test data. This is encouraging for analytical estimation of service failure fatigue crack growth lives.

7. The overall appearances of fatigue fractures were probably controlled by the maximum extent of crack tip cyclic plasticity, which for block programme loading was determined by the largest load excursion per flight block. This implies that below-transition constant amplitude fatigue crack growth rate data and the constant amplitude threshold stress intensity factor range, ΔK_{th}, should not be used to predict fatigue crack growth under variable amplitude loading.

Acknowledgement

This investigation was carried out mainly under contract with the Scientific Research Division of the Directorate of Materiel, Royal Netherlands Air Force.

References

1. H.D. Dill and C.R. Saff, "Environment-load interaction effects on crack growth", Air Force Flight Dynamics Laboratory Report AFFDL-TR-78-137, November 1978.

2. C.R. Saff, "Environment-load interaction effects on crack growth in landing gear steels", Naval Air Development Centre Report NADC-79095-60, December 1980.

3. R.J.H. Wanhill, "Microstructural influences on fatigue and fracture resistance in high strength structural materials", Engineering Fracture Mechanics, Vol. 10, pp. 337-357 (1978).

4. R.O. Ritchie and J.F. Knott, "Mechanisms of fatigue crack growth in low alloy steel", Acta Metallurgica, Vol. 21, pp. 639-648 (1973).

5. A.U. de Koning, "Crack growth prediction methods", NLR Report TR 84121 L, December 1984.

6. G.M. van Dijk, "Statistical load data processing", Advanced Approaches to Fatigue Evaluation, NASA SP-309, pp. 565-598 (1972).

7. G. Glinka, C. Robin, G. Pluvinage and C. Chehimi, "A cumulative model of fatigue crack growth and the crack closure effect", International Journal of Fatigue, Vol. 6, pp. 37-47 (1984).

8. G.R. Yoder, L.A. Cooley and T.W. Crooker, "A critical analysis of grain-size and yield-strength dependence of near-threshold fatigue-crack growth in steels", Naval Research Laboratory Memorandum Report 4576, July 1981.

9. H.L. Ewalds and R.J.H. Wanhill, Fracture Mechanics, Edward Arnold, p. 282 (1984).